Supplemental information

Mapping intratumoral myeloid-T cell interactomes at single-cell resolution reveals targets for overcoming checkpoint inhibitor resistance

Kate Bridges, Gabriela A. Pizzurro, Alev Baysoy, Janani P. Baskaran, Ziyan Xu, Varsha Mathew, Victoria Tripple, Michael LaPorte, Koonam Park, William Damsky, Harriet Kluger, Rong Fan, Susan M. Kaech, Marcus W. Bosenberg, Kathryn Miller-Jensen

Figure S1: Treatment-induced changes in size, cell type composition, and phenotype in 8 day YR1.7 tumors

A

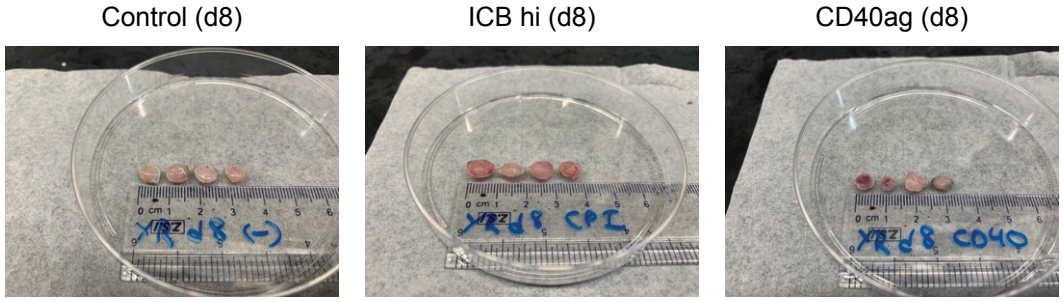

B

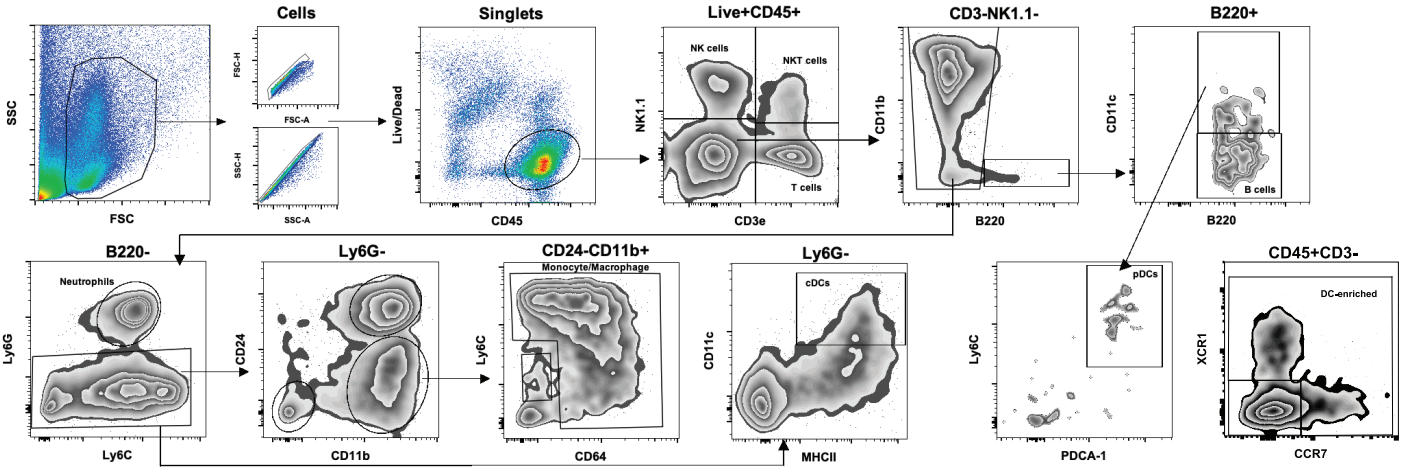

C

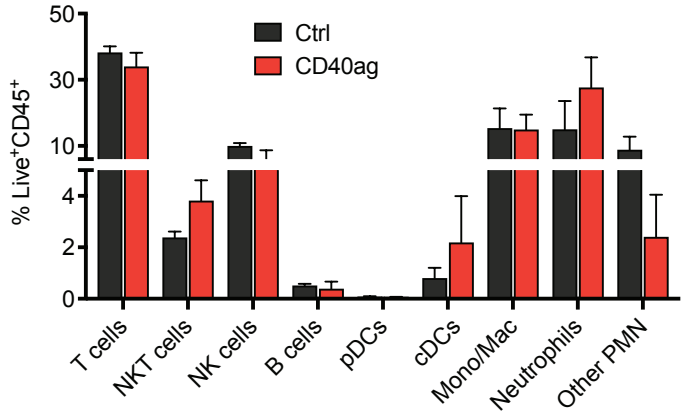

Related to Fig. 1. (A) Images of individual 8 day YR1.7 tumors either left untreated (left), or treated with ICB hi (center) or CD40ag monotherapy (right) 24 hours prior to excision.
(B) Flow cytometry gating strategy for analyzing immune populations in YUMMER1.7 tumors.
(C) Bar graphs describing quantification of immune populations as sorted in (B) from control (black) and CD40ag-treated (red) tumors as a percentage of total Live^{+}CD45^{+} cells. Data is represented as mean ± SEM.

Figure S2: Gene expression patterns were consistent across replicate tumors, confirmed cell types immediately downstream of therapy

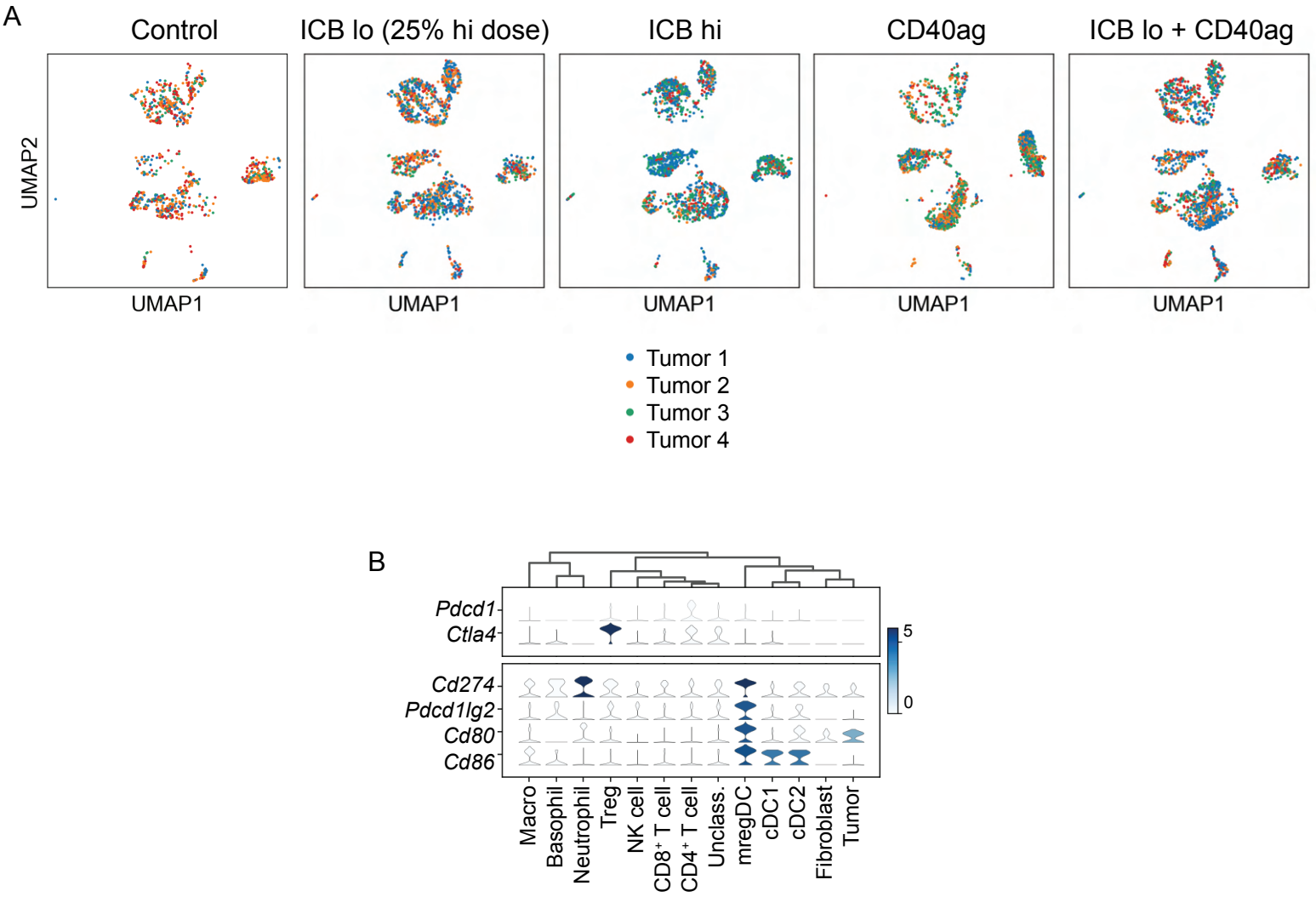

Related to Fig. 2. (A) UMAP embedding of control, ICB lo-treated, ICB hi-treated, CD40ag-treated, and ICB lo + CD40ag-treated scRNA-seq samples separated by treatment condition and colored by individual tumor (4 tumors per group). Single cells from identically-treated tumors were generally well-mixed in two-dimensional space.
(B) Expression of genes which encode for ICB targets (top) and their cognate ligands (bottom) across scRNA-seq samples by cell type.

Figure S3: NICHES and Milo uncover similar axes of acute myeloid-T cell crosstalk across tumor models treated with CD40ag monotherapy

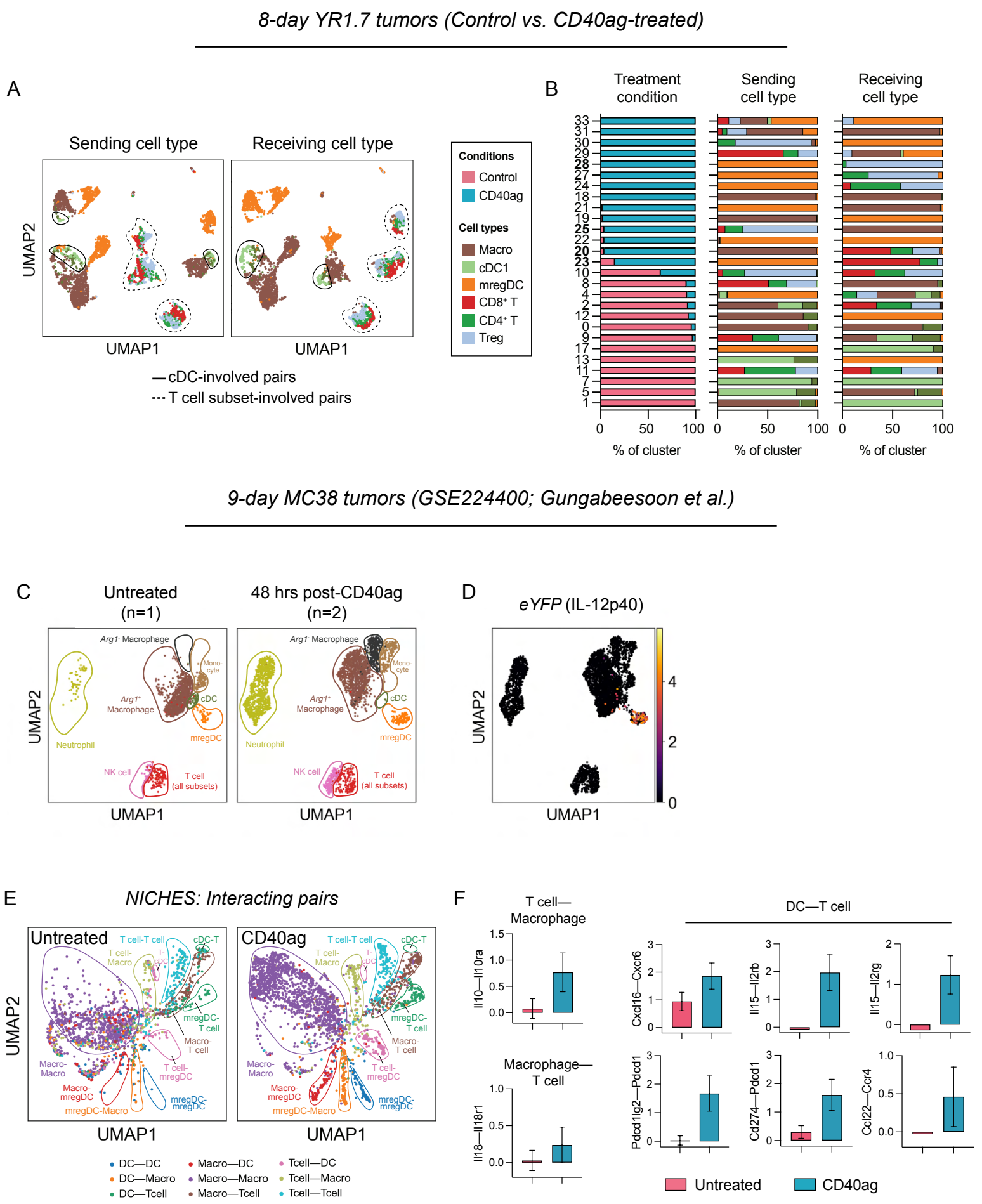

Related to Fig. 3. (A) Integrated UMAP embedding of NICHES interactomes in Fig. 3A colored by sending (left) and receiving (right) cell subset.
(B) Stacked bar graph summarizing the cell-cell pairs which make up each differentially abundant cluster in Fig. 3C by (left) treatment condition, (center) sending cell type, and (right) receiving cell type.
(C) UMAP embedding of publicly available scRNA-seq data (GSE224400) of untreated (left) and CD40ag-treated (right) MC38 tumors 9 days post-tumor initiation and 48 hours post-treatment where applicable. Data is colored by cell type annotations from the original publication.
(D) UMAP embedding as in (C) colored by expression of eYFP (IL-12p40).
(E) UMAP embedding of NICHES interactomes for control (n=1 tumor) and CD40ag monotherapy-treated (n=2 tumors) MC38 samples colored by broad cell type pair. Tumors were collected 9 days post-inoculation and 48 hours post-treatment where applicable.
(G) Bar graphs comparing predicted interaction scores across untreated (pink) and CD40ag monotherapy-treated (blue) T cell-macrophage (top left), macrophage-T cell (bottom left), and DC-T cell (right) pairs for selected ligand-receptor axes. Bar graphs are represented as mean interaction score ± 95% CI (calculated with GraphPad).

Figure S4: ICB rewires myeloid-T cell signaling and cell subset abundance within 24 hours of treatment

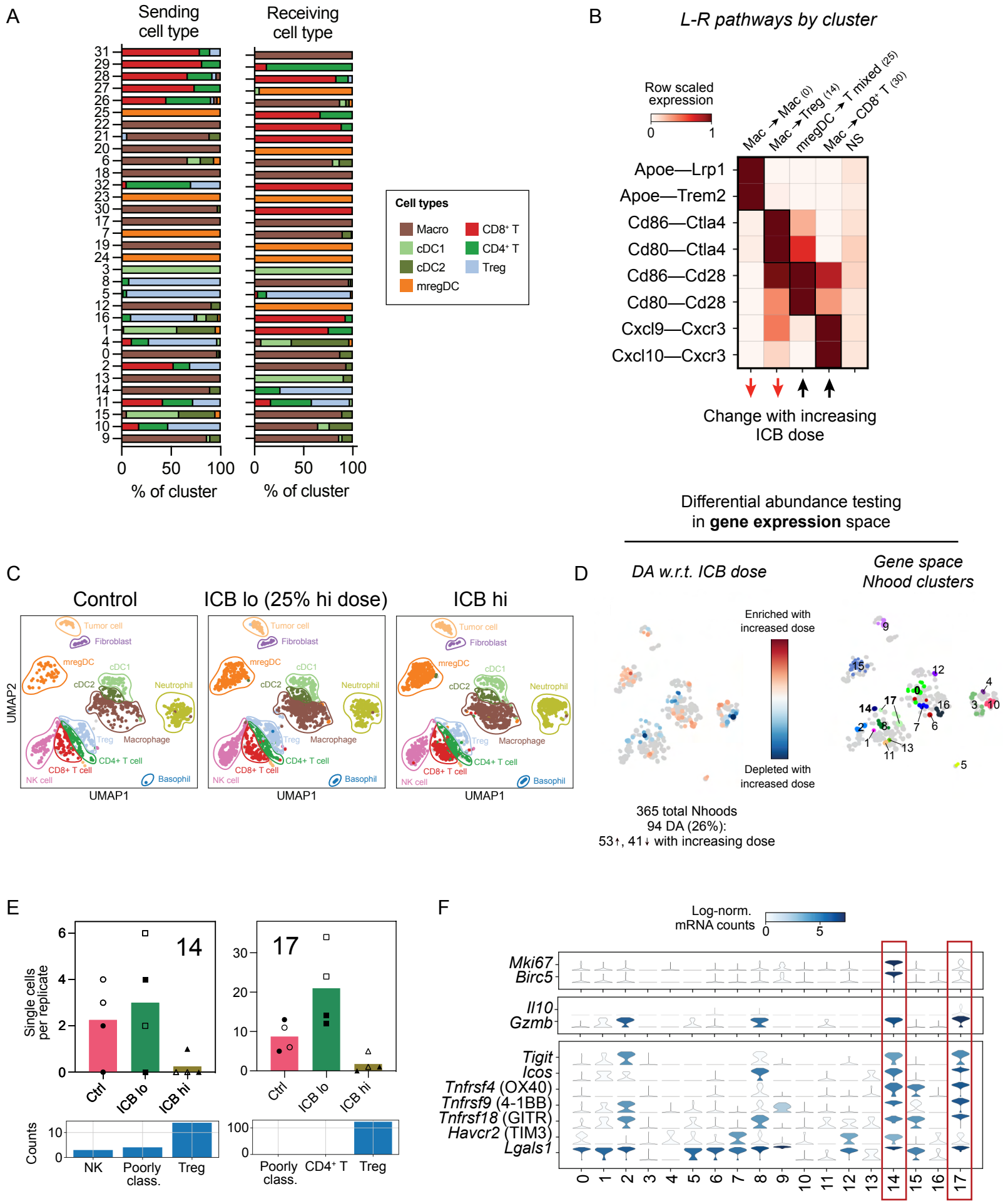

Related to Fig. 4. (A) Stacked bar graphs summarizing the cell-cell pairs which make up each differentially abundant cluster in Fig. 4C by sending cell type (left) and receiving cell type (right).
(B) Heatmap of per-row scaled interaction scores for selected differentially predicted ligand-receptor axes (y-axis) across clusters 0, 14, 25, and 30 and compared to all non-DA neighborhoods (i.e., NS) (x-axis).
(C) UMAP embedding of control (left), ICB lo-treated (center), and ICB hi-treated (right) samples (n=4 tumors per group) separated by treatment condition and colored by cell type as assigned by a neural network-base classifier.
(D) UMAP embedding of (left) 365 Milo-assigned 'neighborhoods' (nhoods) of single cells colored by differential abundance result w.r.t. ICB dose, and of (right) DA nhoods (n=94) colored by grouping for downstream analyses. Grey nhoods were not DA (n=271), while blue (n=41) and red n=53) nhoods decreased and increased in frequency, respectively, with ICB dose.
(E) Bar graphs summarizing number of single cells averaged across replicates (y-axis) per treatment (x-axis) (top) and distribution of annotated cell types (bottom) for DA clusters 14 and 17. Markers distinguish tumor samples from different mice (n=2 per experimental group).
(F) Expression of proliferation markers *Mki67* and *Birc5* (top), immunosuppressive signal-encoding genes *Il10* and *Gzmb* (middle), and immune checkpoints *Tigit, Icos, Tnfrsf4, Tnfrsf9, Tnfrsf18, Havcr2,* and *Lgals1*. Violin shape represents the distribution of gene expression across single cells in each cluster, while the color fill represents average gene expression of each gene across each cluster.

Figure S5: Immunotherapy differentially alters immune composition and relative spatial orientation in the TME

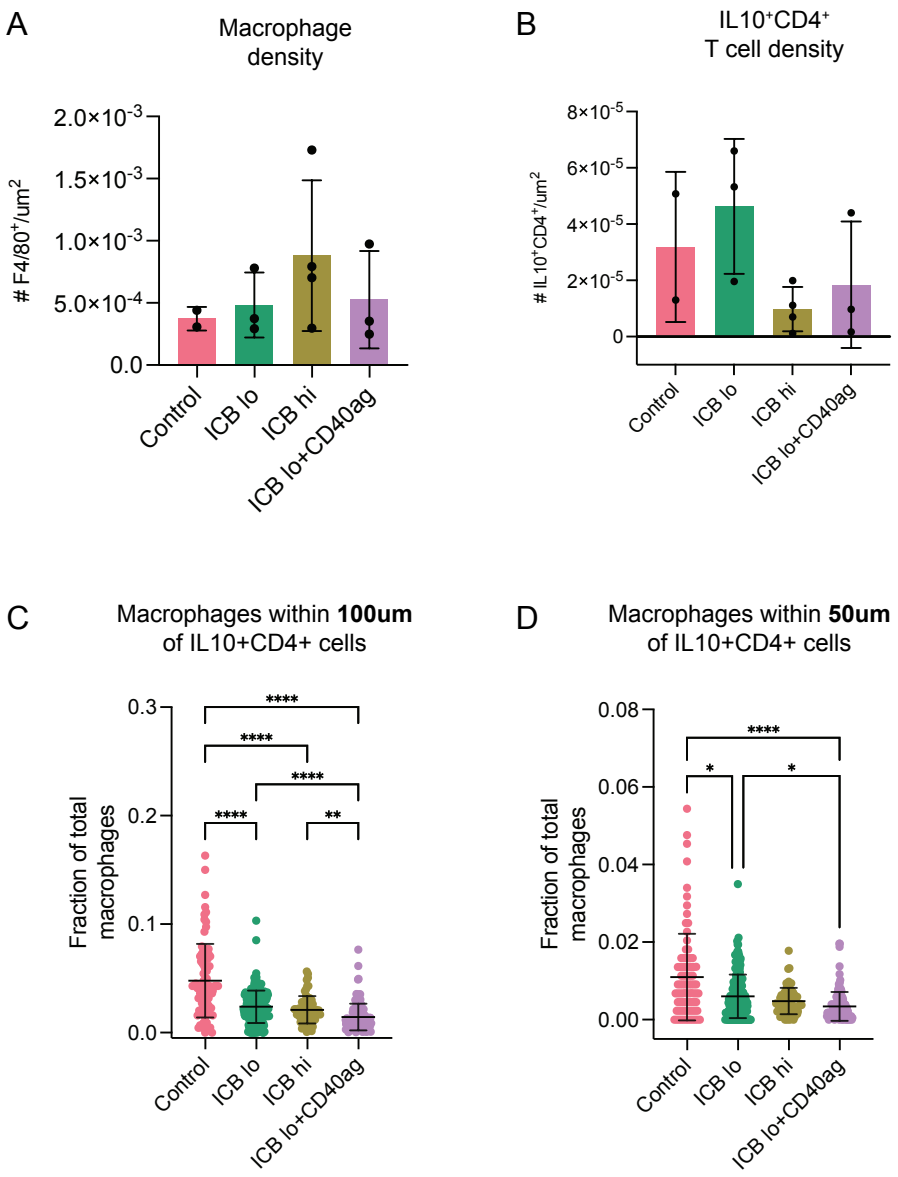

Related to Fig. 4. (A-B) Bar graphs demonstrating quantification of (A) $CD4^+IL\text{-}10^+$ T cell and (B) macrophage ($F4/80^+$) density (absolute number of cells divided by tumor area [um^2])from control (pink), ICB lo- (green), ICB hi- (yellow), and ICB lo + CD40ag-treated (purple) tumor slices (n=2-4 regions from 1 tumor per treatment condition). Summary data is presented as mean ± SD.
(C-D) Scatter plots demonstrating the fraction of total macrophages ($F4/80^+$) within (C) 100 um and (D) 50 um of CD4+IL-10+ T cells from control (pink), ICB lo- (green), ICB hi- (yellow), and ICB lo + CD40ag-treated (purple) tumor slices. Summary data is presented as mean ± SD. ****$p < 0.0001$ by Kruskal-Wallis test (calculated in GraphPad).

Figure S6: NICHES + Milo identify axes of cell-cell communication specific to combinatorial therapy

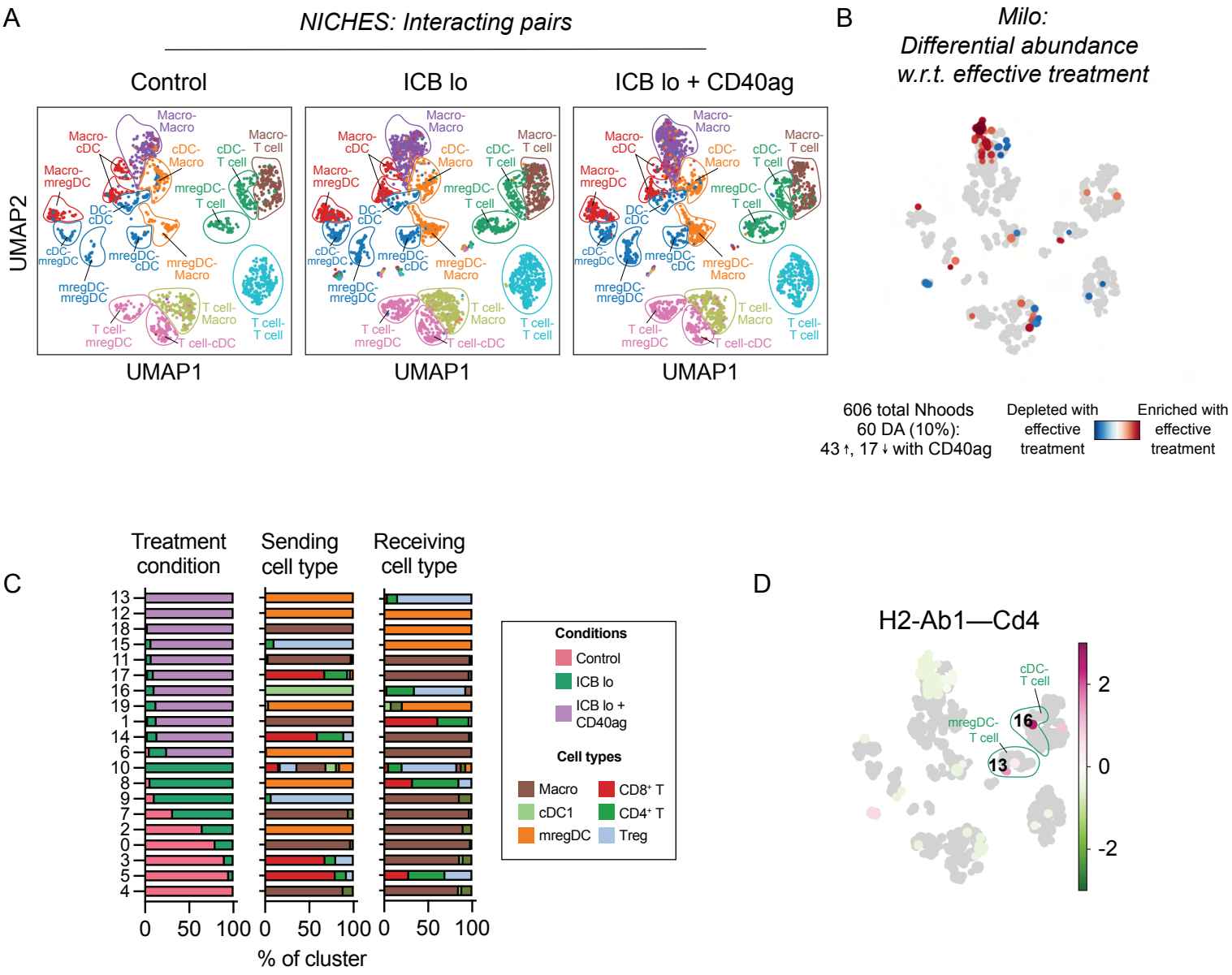

Related to Fig. 5. (A) UMAP embeddings of NICHES interactomes from control, ICB lo- and ICB lo + CD40ag-treated samples separated by treatment condition and colored by broad cell type pair; and (B) UMAP embedding of 606 Milo-assigned 'neighborhoods' (nhoods) of cell-cell pairs colored by differential abundance result w.r.t. effective treatment [i.e., Control, ICB lo = ineffective (0); ICB lo + CD40ag = effective (1)]. Grey nhoods were not differentially abundant (n=546), while blue (n=17) and red (n=43) nhoods decreased and increased in frequency, respectively, with effective treatment. (C) Stacked bar graphs summarizing the cell-cell pairs which make up each differentially abundant cluster in Fig. 5A by treatment condition (left), sending cell type (center), and receiving cell type (right). (D) UMAP embedding as in (A) colored by predicted interaction score along H2-Ab1 – Cd4 as averaged across single cell-cell pairs in each nhood.

Figure S7: CD40ag-induced IL-12 signaling impacts acute trends in tumor growth but not long-term survival

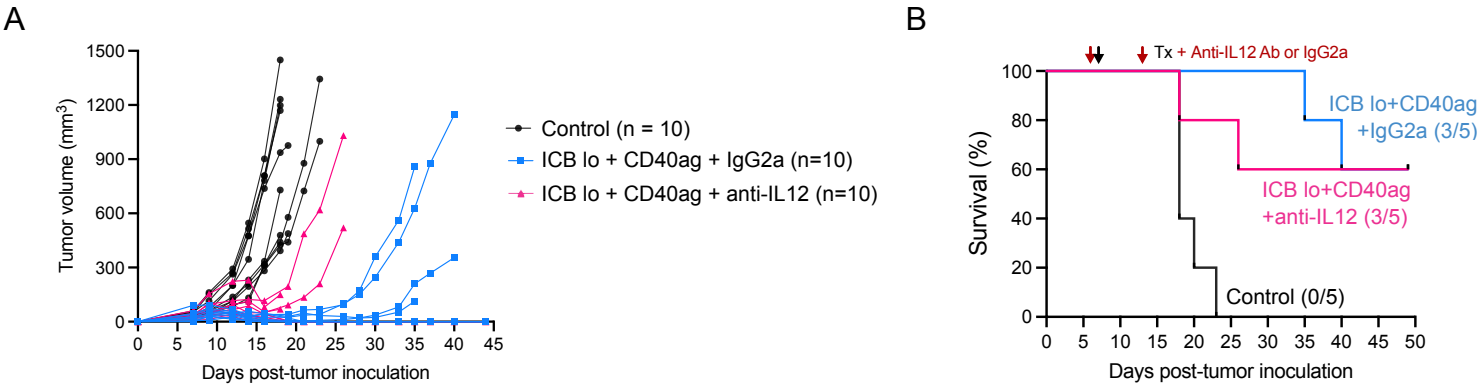

Related to Fig. 5. (A) Tumor volume (mm^3) curves over time for YUMMER1.7-bearing mice (2 tumors per mouse) either left untreated (n=10), treated with ICB lo + CD40ag + IgGa (n=10), or treated with ICB lo + CD40ag + IL-12 blockade (n=10).
(B) Corresponding Kaplan-Meier survival curves for tumor volume data shown in (A).

Figure S8: CD40ag in combination with ICB primarily alters myeloid heterogeneity

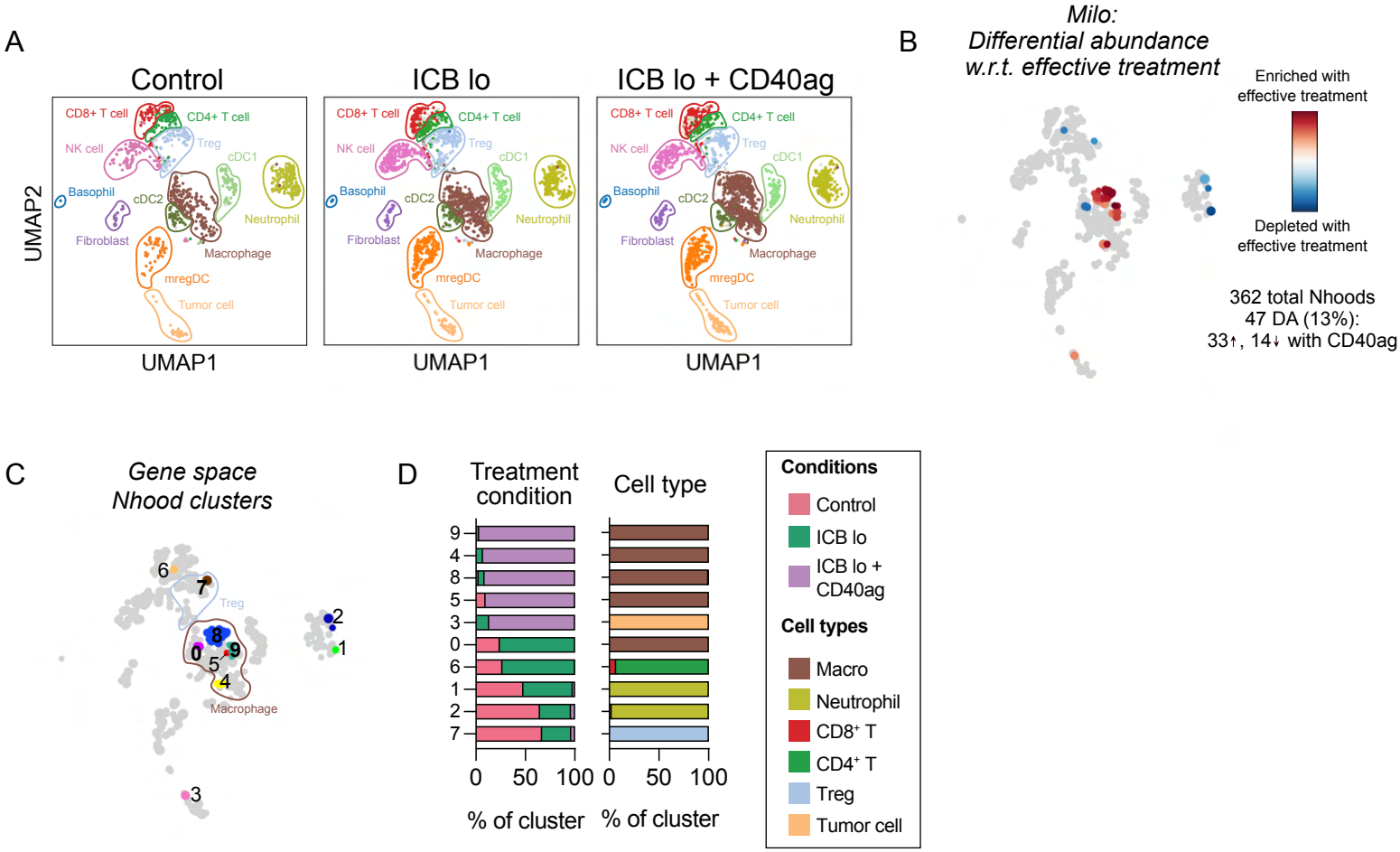

Related to Fig. 5. (A) UMAP embedding of control (left), ICB lo-treated (center), and ICB lo+CD40ag-treated (right) samples (n=4 tumors per group) separated by treatment condition and colored by cell type as assigned by a neural network-based classifier.
(B) UMAP embedding as in (A) of 362 Milo-assigned 'neighborhoods' (nhoods) of single cells colored by differential abundance result w.r.t. effective treatment [i.e., Control, ICB lo = ineffective (0);
ICB lo + CD40ag = effective (1)]. . Grey nhoods were not DA (n=315), while blue (n=14) and red (n=33) nhoods decreased and increased in frequency, respectively, with effective treatment.
(C) UMAP embedding of as in (B) of DA nhoods (n=47) colored by grouping for downstream analyses.
(D) Stacked bar graphs summarizing the cells which make up each differentially abundant cluster in (C) by treatment condition (left) and cell type (right).

Figure S9: Blocking IL-12/IL-18 signaling alters peripheral blood secretion activated by combinatorial therapy

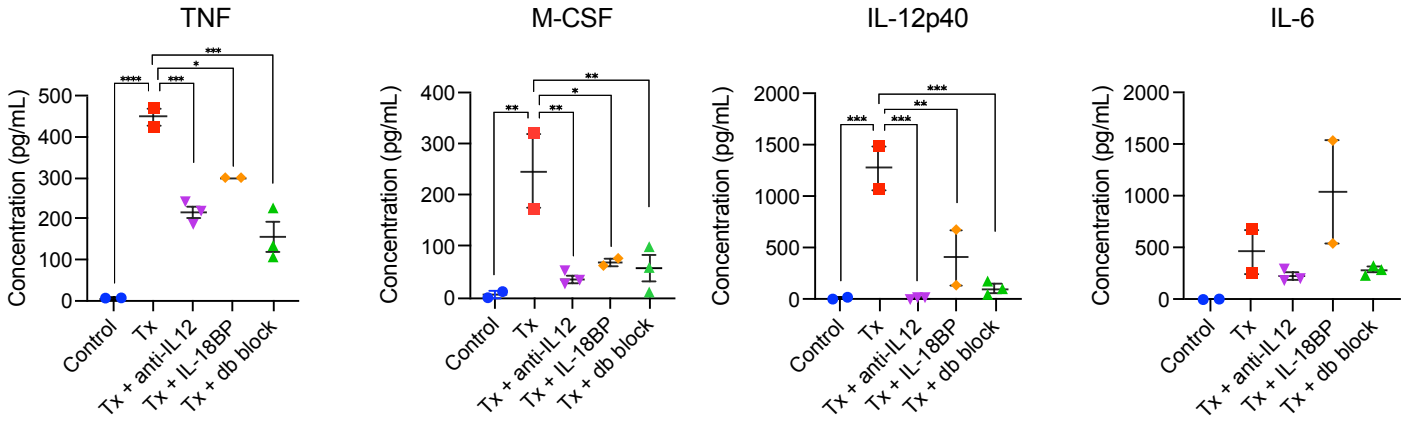

Related to Fig. 5. Example plots of peripheral blood cytokine expression levels in YUMMER1.7-bearing mice for TNF, M-CSF, IL-12p40, and IL-6. Mice were either left untreated (blue) or were treated with ICB lo + CD40ag (abbrev. Tx, red), Tx + anti-IL12 (purple), Tx + IL-18BP (orange), or Tx + anti-IL12 + IL-18BP ('db block', green). Summary data is presented as mean ± SEM. *p < 0.05, **p < 0.01, ***p < 0.001, ***p < 0.0001 by ordinary one-way ANOVA with Dunnett's multiple comparisons testing (calculated in GraphPad). Only showing significant results for comparisons between Tx and other conditions.

Fig. S10: Macrophages and DCs do not colocalize similarly with T cell subsets 24 hours post-therapy

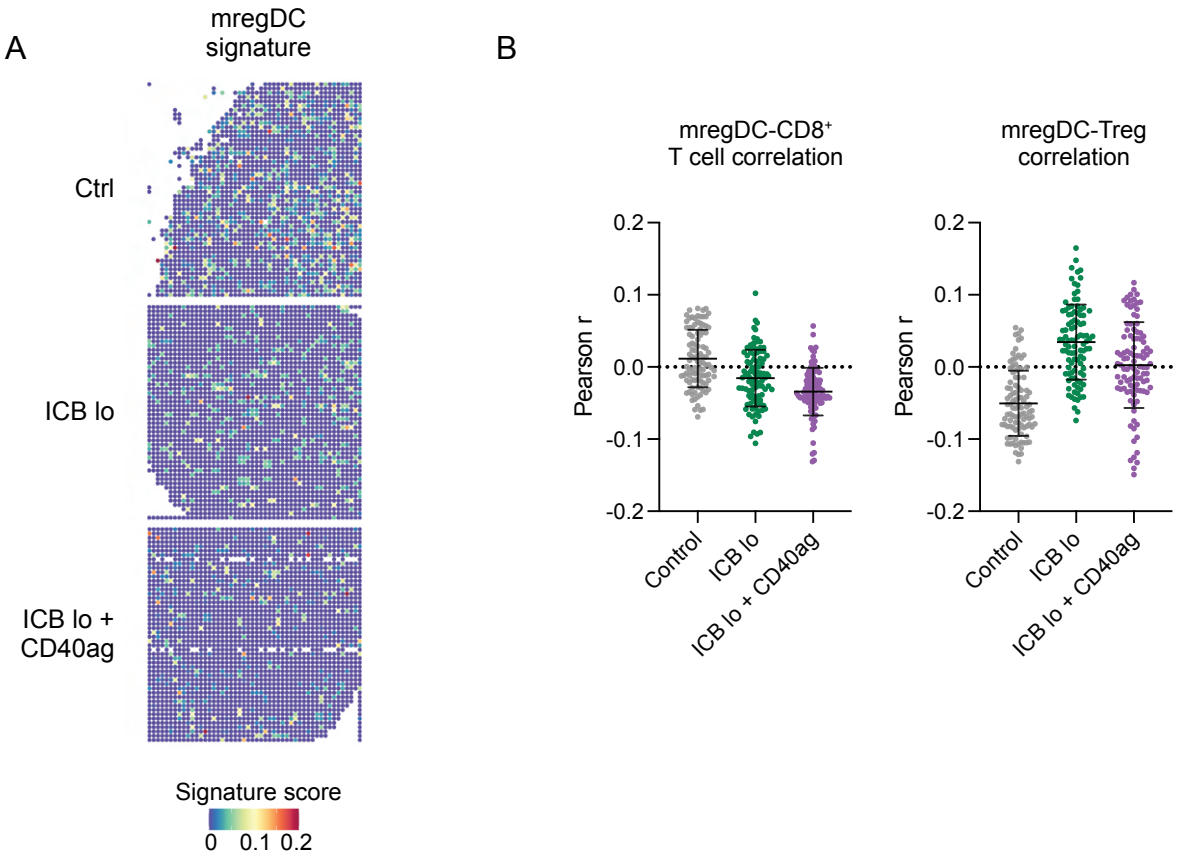

Related to Fig. 6. (A) mregDC signature scores for each pixel in the spatial transcriptomics spot map. (B) Scatter plots demonstrating per-pixel Pearson product-moment correlation coefficients between (left) mregDC and $CD8^+$ T cell signature scores and (right) mregDC and Treg signature scores for 100 20x20 grids randomly sampled from each DBiT-seq sample (control – grey, ICB lo – green, ICB lo + CD40ag – purple). Summary data is presented as mean ± SD.

Table S1. Summary of all differentially abundant neighborhood clusters in Fig. 5A.

Cluster no.	Enriched for:	Sending cell type	Receiving cell type	Key signaling axes	Hypothesized function	Supporting references
0	Untreated	Macrophage	Macrophage	Apoe—Trem2 Spp1—Cd44	Anti-inflammatory macrophage activation, tumor growth, anti-PD-1 resistance	[1,2]
1	Tx	Macrophage	$CD8^+$/ $CD4^+$ T	Described in Fig. 5		
2	Untreated	mregDC	Macrophage	Ccl5—Ccr(1,5) Cx3cl1—Cx3cr1	Chemotaxis, myeloid infiltration into the TME	[3]
3	Untreated	Mixed T cell	Macrophage	Ifng—Ifngr(1,2) Adam10—Trem2 Cd47—Sirpa	Dual pro- and anti-inflammatory macrophage polarization	[4]
4	Untreated	Macrophage	Macrophage	Ccl12—Ccr2 Ccl7—Ccr(1, 2,5)	Monocyte/macrophage recruitment into the tumor	[5,6]
5	Untreated	$CD8^+$ T	Mixed T cell	Ifng—Ifngr1 Cd274—Pdcd1	Suppression of T cell proliferation and IFNg production, tumor tolerance	[7]
6	Tx	mregDC	Macrophage	Ccl5—Ccr(1,5) Anxa2—Tlr2	Chemotaxis, proinflammatory macrophage polarization, proinflammatory interleukin secretion	[8]
7	ICB lo	Macrophage	Macrophage	Apoe—Trem2 C3—C3ar1	Anti-inflammatory macrophage activation, regulation of TIM-3 expression	[1,9]
8	ICB lo	mregDC	Mixed T cell	Cxcl16—Cxcr6 Cd80/86—Cd28 Il15—Il2r(b,g)	Positioning and survival of CTLs, sustained tumor control	[10]

9	ICB lo	Treg	Macrophage	Described in Fig. 5		
10	ICB lo	Mixed	Mixed	-	-	-
11	Tx	Macrophage	Macrophage	Ccl2—Ccr2 Ccl(2,4, 12)—Ccr(1,5)	Chemotaxis, myeloid infiltration into the TME, macrophage maturation	[11]
12	Tx	mregDC	mregDC	Sema7a—Itgb1	DC migration	[12]
13	Tx	mregDC	Treg	Described in Fig. 5		
14	Tx	$CD8^+/CD4^+$ T	Macrophage			
15	Tx	Treg	mregDC			
16	Tx	cDC1	Mixed T cell	Described in Fig. S6		
17	Tx	$CD8^+/CD4^+$ T	Macrophage	Ccl5—Ccr(1,5) Adam10—Trem2 Cd47—Sirpa	T cell survival, modulation of phagocytosis	[13,14]
18	Tx	Macrophage	mregDC	Il18—Cd48 Fn1—Cd44	Chemotaxis, cell-cell adhesion	[15–17]
19	Tx	mregDC	mregDC	Sema7a—Itgb1	DC migration	[12]

Supplementary references

1. Molgora, M., Esaulova, E., Vermi, W., Hou, J., Chen, Y., Luo, J., Brioschi, S., Bugatti, M., Omodei, A.S., Ricci, B., et al. (2020). TREM2 Modulation Remodels the Tumor Myeloid Landscape Enhancing Anti-PD-1 Immunotherapy. Cell *182*, 886-900.e17. https://doi.org/10.1016/j.cell.2020.07.013.
2. Zhao, Y., Huang, Z., Gao, L., Ma, H., and Chang, R. (2024). Osteopontin/SPP1: a potential mediator between immune cells and vascular calcification. Front. Immunol. *15*. https://doi.org/10.3389/fimmu.2024.1395596.
3. Ishida, Y., Kuninaka, Y., Yamamoto, Y., Nosaka, M., Kimura, A., Furukawa, F., Mukaida, N., and Kondo, T. (2020). Pivotal Involvement of the CX3CL1-CX3CR1 Axis for the Recruitment of M2 Tumor-Associated Macrophages in Skin Carcinogenesis. Journal of Investigative Dermatology *140*, 1951-1961.e6. https://doi.org/10.1016/j.jid.2020.02.023.
4. Al-Sudani, H., Ni, Y., Jones, P., Karakilic, H., Cui, L., Johnson, L.D.S., Rose, P.G., Olawaiye, A., Edwards, R.P., Uger, R.A., et al. (2023). Targeting CD47-SIRPa axis shows potent preclinical anti-tumor activity as monotherapy and synergizes with PARP inhibition. npj Precis. Onc. *7*, 1–10. https://doi.org/10.1038/s41698-023-00418-4.
5. Unver, N. (2019). Macrophage chemoattractants secreted by cancer cells: Sculptors of the tumor microenvironment and another crucial piece of the cancer secretome as a therapeutic target. Cytokine & Growth Factor Reviews *50*, 13–18. https://doi.org/10.1016/j.cytogfr.2019.05.010.
6. Wu, Z., Bai, X., Lu, Z., Liu, S., and Jiang, H. (2022). LINC01094/SPI1/CCL7 Axis Promotes Macrophage Accumulation in Lung Adenocarcinoma and Tumor Cell Dissemination. J Immunol Res *2022*, 6450721. https://doi.org/10.1155/2022/6450721.
7. Zheng, Y., Han, L., Chen, Z., Li, Y., Zhou, B., Hu, R., Chen, S., Xiao, H., Ma, Y., Xie, G., et al. (2022). PD-L1+CD8+ T cells enrichment in lung cancer exerted regulatory function and tumor-promoting tolerance. iScience *25*, 103785. https://doi.org/10.1016/j.isci.2022.103785.
8. Andersen, B.M., Xia, J., Epstein, A.L., Ohlfest, J.R., Chen, W., Blazar, B.R., Pennell, C.A., and Olin, M.R. (2016). Monomeric annexin A2 is an oxygen-regulated toll-like receptor 2 ligand and adjuvant. j. immunotherapy cancer *4*, 11. https://doi.org/10.1186/s40425-016-0112-6.
9. Yang, H., Li, L., Liu, X., and Zhao, Y. (2021). High Expression of the Component 3a Receptor 1 (C3AR1) Gene in Stomach Adenocarcinomas Infers a Poor Prognosis and High Immune-Infiltration Levels. Med Sci Monit *27*, e927977-1-e927977-14. https://doi.org/10.12659/MSM.927977.
10. Di Pilato, M., Kfuri-Rubens, R., Pruessmann, J.N., Ozga, A.J., Messemaker, M., Cadilha, B.L., Sivakumar, R., Cianciaruso, C., Warner, R.D., Marangoni, F., et al. (2021). CXCR6 positions cytotoxic T cells to receive critical survival signals in the tumor microenvironment. Cell *184*, 4512-4530.e22. https://doi.org/10.1016/j.cell.2021.07.015.
11. Kaufmann, A., Salentin, R., Gemsa, D., and Sprenger, H. (2001). Increase of CCR1 and CCR5 expression and enhanced functional response to MIP-1α during differentiation of human monocytes to macrophages. Journal of Leukocyte Biology *69*, 248–252. https://doi.org/10.1189/jlb.69.2.248.
12. van Rijn, A., Paulis, L., te Riet, J., Vasaturo, A., Reinieren-Beeren, I., van der Schaaf, A., Kuipers, A.J., Schulte, L.P., Jongbloets, B.C., Pasterkamp, R.J., et al. (2016). Semaphorin 7A Promotes Chemokine-Driven Dendritic Cell Migration. J Immunol *196*, 459–468. https://doi.org/10.4049/jimmunol.1403096.
13. Komori, S., Saito, Y., Nishimura, T., Respatika, D., Endoh, H., Yoshida, H., Sugihara, R., Iida-Norita, R., Afroj, T., Takai, T., et al. (2023). CD47 promotes peripheral T cell survival by preventing dendritic cell–mediated T cell necroptosis. Proceedings of the National Academy of Sciences *120*, e2304943120. https://doi.org/10.1073/pnas.2304943120.
14. Schlepckow, K., Kleinberger, G., Fukumori, A., Feederle, R., Lichtenthaler, S.F., Steiner, H., and Haass, C. (2017). An Alzheimer-associated TREM2 variant occurs at the ADAM cleavage site and affects shedding and phagocytic function. EMBO Molecular Medicine *9*, 1356–1365. https://doi.org/10.15252/emmm.201707672.

15. Fukushima, K., Ikehara, Y., and Yamashita, K. (2005). Functional Role Played by the Glycosylphosphatidylinositol Anchor Glycan of CD48 in Interleukin-18-induced Interferon-γ Production *. Journal of Biological Chemistry *280*, 18056–18062. https://doi.org/10.1074/jbc.M413297200.
16. Gutzmer, R., Langer, K., Mommert, S., Wittmann, M., Kapp, A., and Werfel, T. (2003). Human Dendritic Cells Express the IL-18R and Are Chemoattracted to IL-18 1. The Journal of Immunology *171*, 6363–6371. https://doi.org/10.4049/jimmunol.171.12.6363.
17. Termeer, C., Johannsen, H., Braun, T., Renkl, A., Ahrens, T., Denfeld, R.W., Lappin, M.B., Weiss, J.M., and Simon, J.C. (2001). The role of CD44 during CD40 ligand-induced dendritic cell clustering and maturation. Journal of Leukocyte Biology *70*, 715–722. https://doi.org/10.1189/jlb.70.5.715.